# Chapter 16

# High-Throughput Label-Free Detection of DNA Hybridization and Mismatch Discrimination Using Interferometric Reflectance Imaging Sensor

**Sunmin Ahn, David S. Freedman, Xirui Zhang, and M.Selim Ünlü**

## Abstract

Optical label-free biosensors have demonstrated advantages over fluorescent-based detection methods by allowing accurate quantification while also being capable of measuring dynamic bimolecular interactions. A simple, high-throughput, solid-phase, and label-free technique, interferometric reflectance imaging sensor (IRIS), can quantify the mass density of DNA with pg/mm$^2$ sensitivity by measuring the optical path difference. We present the design of the IRIS instrument and complementary microarrays that can be used to perform a quantitative analysis of DNA microarrays. Finally, we present methods to accurately calculate the hybridization efficiency and identify SNPs from dynamic measurements, as well as supporting software algorithms needed for robust data processing.

**Key words** DNA microarrays, Label-free detection, Optical interferometry, Hybridization, SNP, High-throughput analysis, Quantitative analysis, Spot finding

## 1 Introduction

In the past two decades, advancements in biotechnology have provided us with unprecedented amounts of genomic data. In particular, DNA microarrays have been widely used in biological and medical research. The high-throughput capacity of DNA microarrays provides an enormous economic advantage in genomic analysis. Label-free biosensors are creating additional advancements in biotechnology, and interest in label-free sensing has grown exponentially [1]. This growth is driven by several advantages over traditional fluorescence-based sensing. These advantages include reduced cost and preparation time with the elimination of the labeling step, more accurate observation of molecular interaction in their native states, and the ability to provide quantitative measurements. Quantitative analysis is difficult with fluorescent techniques because of the heterogeneity in labeling efficiency and noncontrolled photobleaching. An additional advantage of

Dmitry M. Kolpashchikov and Yulia V. Gerasimova (eds.), *Nucleic Acid Detection: Methods and Protocols*,
Methods in Molecular Biology, vol. 1039, DOI 10.1007/978-1-62703-535-4_16, 

label-free sensing is the ability to dynamically monitor molecular interactions, consequently, providing information on binding kinetics. Real-time kinetic measurements are not available through conventional labeling approach because the detection must occur after the non-reacted reporting molecules have washed off the sensor. Thus, developing applications for high-throughput label-free detection of DNA microarrays are of great interest.

One such application is the detection of single-nucleotide polymorphisms (SNPs). Genetic variations caused by SNPs occur as often as every few hundred base pairs in genomic DNA [2, 3]. Many SNPs have been identified as important biomarkers [4, 5]. Thus, successful detection of SNPs will expedite advancements in personalized medicines as well as the diagnosis and treatment of hereditary diseases. A common method for genotyping of SNPs uses MALDI-TOF MS (matrix assisted laser desorption/ionization time of flight mass spectrometry), but samples are usually labeled with mass tags [6], and mass spectrometry is generally only capable of very limited throughput. While there have been efforts to increase throughput for SNP detection for MALDI-TOF MS-based methods, the throughput offered has yet to achieve the multiplexing capability of microarrays [7]. Very few SNP genotyping solutions offer high-throughput capabilities by using microarrays [8, 9], but these techniques require labeling the targets. In general, these systems can be very expensive, bulky, and complex, and their utilization requires complicated sample preparation. Most importantly, they do not offer quantitative expression analysis [5]. A few label-free sensors have demonstrated SNP detection, but these systems are rather difficult to implement. For example, they require enzymatic reactions on sensors, demand precise control of the environment (i.e., temperature), and present limited throughput [10–12]. Thus, there is an increasing demand for SNP genotyping and gene expressions technology that is simple, cost-effective, quantitative, and amenable to automated high-throughput analysis.

Recently, we introduced a biosensor, interferometric reflectance imaging sensor (IRIS), for high-throughput label-free detection of biomolecular interactions on a glass surface with a buried reference plane [13, 14]. The detection principle of IRIS is summarized in Fig. 1. We have demonstrated label-free detections of

**Fig. 1** (continued) changes of five different probe oligonucleotides are plotted. The data shown is the average of 15 spots per probe type ($T_1$P: positive control, complementary to $T_1$, $T_1$N: negative control, noncomplementary to $T_1$, $T_2$PM: perfect match probe, perfectly complementary to $T_2$, $T_2$MM: mismatch probe, single point mutation to $T_2$PM, $T_2$DM: double mismatch probe, two point mutations to $T_2$PM). A brief overview of the experiment is given. Target 1 ($T_1$, 40mer ssDNA) is introduced ($t$=40 min), and the wash buffer ($t$=100 min) washes away weakly interacting duplexes. Only the probes that are complementary to $T_1$ remain hybridized as indicated by ~2.5 ng/mm$^2$ mass increase on $T_1$P. When deionized water ($ddH_2O$) is introduced, all duplexes denature, and the surface is regenerated. Target 2 ($T_2$, 20mer ssDNA) is introduced ($t$=190 min), and probes that are complementary to $T_2$ ($T_2$PM, $T_2$MM, $T_2$DM) show similar mass increase regardless of the presences of mutations. Probes with double mutations start denaturing with the introduction of the wash buffer ($t$=260 min). When a buffer with much weaker ionic strength (0.5 mM [$Na^+$]) is introduced, all probes start denaturing, and different probe types display different denaturation kinetics. This figure was adapted from ref. [14] with permission from Elsevier

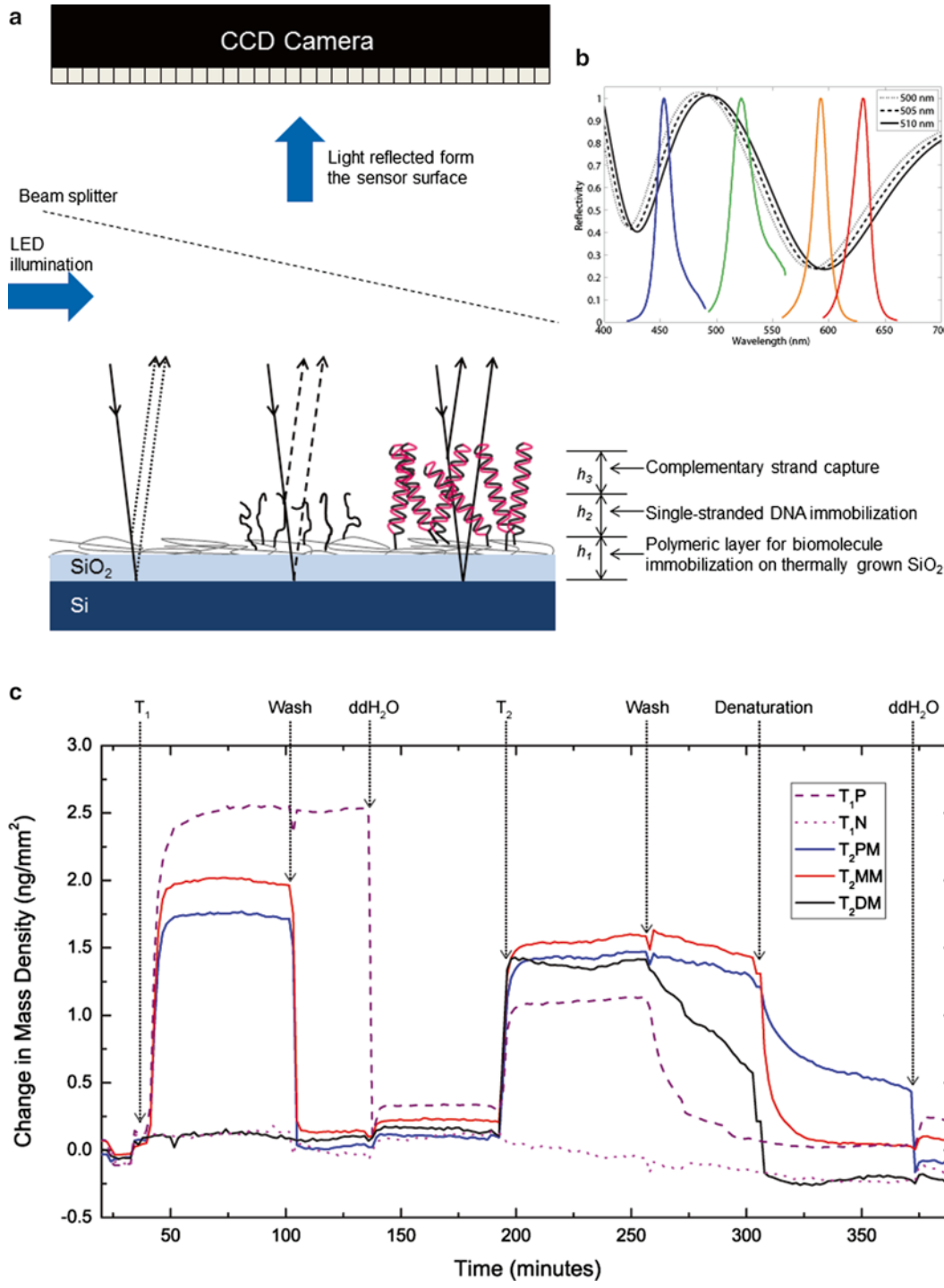


**Fig. 1** Schematic representation of label-free detection of DNA microarray. (**a**) Detection principle of IRIS is shown. DNA microarray on a $SiO_2$–Si-layered substrate is illuminated with multiple wavelengths, and microarray images are acquired with a CCD camera. The interference of reflected light from the interfaces of the layered substrate, air–$SiO_2$ (or buffer–$SiO_2$) and $SiO_2$–Si, results in varied intensity as a function of wavelength, as illustrated in (**b**). A functional polymeric surface is used to specifically immobilize DNA on the surface ($h_1$). Accumulation of biomolecules on the surface changes the optical path length ($h_2$ and $h_3$), causing a quantifiable optical phase shift in the reflected intensity. The spectral shift of the reflectance is measured allowing one to calculate the optical path difference assuming that the refractive index of the DNA is the same as $SiO_2$ [13]. (**c**) A typical result obtained by dynamic detection of DNA hybridization and denaturation is shown. The surface mass density

protein–protein, protein–virus, DNA–DNA, and DNA–protein interactions [13–17] with ~10 pg/mm$^2$ noise floor during dynamic detection [13]. In particular, we have shown that IRIS is capable of high-throughput quantitative analysis of DNA microarrays by comparing immobilized oligonucleotide mass density before and after hybridization [16]. While hybridization signal was well above the noise floor, the level of mass increase upon hybridization was not an ideal way of differentiating the duplexes with perfectly complementary oligonucleotides from duplexes with point mutations. Fish et al. explored hybridization kinetics to detect a single nucleotide mutation, but determining an optimal condition to investigate SNP in a high-throughput manner was difficult [18]. Thus, we exploited the difference in duplex stability by lowering the ionic strength of the buffer while monitoring the denaturation kinetics. We observed a clear difference in the denaturation kinetics of the duplexes with and without a mutation. Therefore, IRIS is a powerful tool for DNA microarray analysis as it allows quantitative analysis for genomic expression and enables SNP detections without additional complex biochemical reactions or precise temperature control (Fig. 1c). Furthermore, IRIS is simple, compact, and easily automated for high-throughput analysis.

In this chapter, we present a comprehensive method on quantitative analysis of DNA hybridization and SNP detection using IRIS. Instructions on building IRIS are given, and the fabrication processes of DNA microarrays are presented in detail. For label-free detection methods, data analysis is a critical step for accurate quantification. An interferometric model is introduced and a method to analyze the biomolecular interactions that take place on the sensor surface is described. Particularly, materials and methods that are required for dynamic detection, such as the flow cell components, as well as data processing and analysis techniques are described in great detail because dynamic detection methods are more complicated than static detection methods. Finally, methods to calculate the hybridization signal and identify SNPs are presented.

## 2 Materials

### 2.1 Interferometric Reflectance Imaging Sensor

#### 2.1.1 Instrument

1. Scientific CCD camera. Retiga-2000R (QImaging, Corp., Surrey, BC, Canada).
2. LED illumination source. ACULED VHL, ACL01-MC-RGYB (Excelitas Technologies, Pfaffenhofen, Germany) (*see* **Note 1**).
3. Microscope objective. 2× Plan Achromatic, 0.06 NA.
4. Beam splitter. Pellicle coated for the visible spectrum.

5. Lenses. Achromatic doublets for the visible spectrum.
6. Diffuser. N-BK7 Ground Glass Diffuser, 220 Grit.
7. Iris diaphragm.
8. Stage. 1/2″ XYZ translation stage.
9. Mechanical components for optical setup. Cage system and lens holders.
10. Data acquisition card.
11. Computer. Acquisition and processing PC with Firewire card and Windows XP operating system.

#### 2.1.2 Substrate

1. Silicon substrate. 100 mm double side polished with 500 nm of thermally grown oxide (Silicon Valley Microelectronics, Inc., Santa Clara, CA, USA).
2. Positive photoresist.
3. Spinner.
4. Mask aligner.
5. Hot plate.
6. Developer.
7. Plasma asher.
8. Dicer.
9. Buffered oxide etch (BOE). 6:1 volume ratio of 40 % $NH_4F$ in water to 49 % HF in water.
10. Photomask. 5-in. green soda-lime substrate with iron oxide.
11. Acetone.

### 2.2 Surface Chemistry

1. Copoly (DMA-NAS-MAPS) (Lucidant Polymers, Sunnyvale, CA, USA) (*see* **Note 2**).
2. Ammonium sulfate solution: aqueous solution of $(NH_4)_2SO_4$ at 40 % saturation level. To prepare a stock solution, add 242 g of ammonium sulfate to 1 L of deionized water.
3. Acetone and methanol.
4. Plastic Petri dish.
5. Plasma asher.
6. Vacuum drying oven.

### 2.3 DNA Microarray Preparation and Hybridization

Prepare spotting buffer and hybridization buffer in 2× concentration. Dilute the buffers to 1× concentration for spotting and hybridization. For buffers, use deionized water filtered with Barnstead Nanopure Diamond water purification system with 18.2 MΩ resistivity setting and a 0.2 μm particle filter.

1. Spotting buffer (2×): 300 mM sodium phosphate buffer, pH 8.5. Prepare 300 mM $Na_2HPO_4$ and adjust the pH to 8.5

with 300 mM $NaH_2PO_4$. The concentration of the final spotting buffer (1×) is 150 mM. Store at room temperature.

2. MES stock buffer (12×): 1.22 M MES, 0.89 M NaCl. To prepare 100 mL of 12× MES stock buffer, add 6.46 g of MES hydrate, 19.3 g of MES sodium salt to 80 mL of deionized water and mix. Adjust pH to 6.5–6.7 with HCl and/or NaOH and bring the volume up to 100 mL. Store at 4 °C.
3. Hybridization buffer (2×): 200 mM MES, 2 M NaCl, 40 mM EDTA. To prepare 50 mL of hybridization buffer (2×), mix 8.3 mL of MES stock buffer (12×), 17.7 mL of 5 M NaCl, 4.0 mL of 0.5 M EDTA, and 20 mL of deionized water. The content of hybridization buffer (1×) is 100 mM MES, 1 M NaCl, 20 mM EDTA. Store at 4 °C.
4. Wash buffer: SSPE solution (6×), 0.01 % Tween-20. Store at room temperature.
5. Blocking solution: 50 mM ethanolamine, 50 mM Tris–HCl, pH 8.5, 150 mM NaCl. Store at room temperature.
6. Microarray spotter.
7. Multipurpose rotating shaker.

### 2.4 Flow Components for Dynamic Detection

Here, we describe the custom made flow cell, as shown in Fig. 2, and all other necessary components for executing a real-time binding experiment.

1. Flow cell.
   (a) Laser grade window (BK7) with less than 5 arc minutes wedge and custom anti-reflection coatings (CVI Melles Griot, Albuquerque, NM) (*see* **Note 3**).
   (b) Gasket: 250 μm thick silicone rubber sheet (*see* **Note 4**).
   (c) The chip holder (*see* **Note 5**).
   (d) Two polyoxymethylene (POM) blocks (*see* **Note 6**).
   (e) Four thumb screws.
2. Millex-GS filter unit with 0.22 μm pore size.
3. Peristaltic pump.
4. Platinum cured silicone tubing (*see* **Note 7**).
5. Lens cleaning tissue.
6. Ethanol and isopropanol.

### 2.5 Software

Label-free biosensors require new methods to process and analyze raw data. Physical artifacts such as dirt and salt, which are difficult to detect by fluorescence-based sensors, are easily detected by label-free biosensors, and they can skew the result. This makes the software used with IRIS a critical component of the entire system. A custom application written in the MATLAB computing

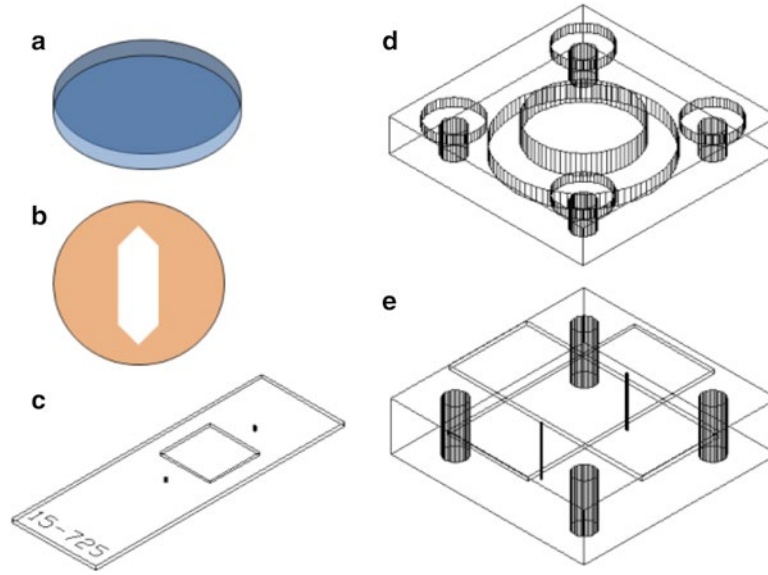


**Fig. 2** Five different components of the flow cell for IRIS are presented. (**a**) BK-7 window with anti-reflection coating on both sides. (**b**) Silicone rubber sheet gasket. (**c**) A custom designed chip holder to keep the IRIS chip in place. (**d**) The top block of the flow cell. It has indents for the windows and thru holes for the screws. (**e**) The bottom block of the flow cell. It has threaded holes for the screws to secure the assembly, and two small thru holes for tubing. The bottom block also has two different layers of indents crossing at a 90° angle. The top indent was designed to fit a chip holder which will place the IRIS chip at the same location for different experiments. The bottom indent was designed to fit a resistive heater to control the temperature of the IRIS chip. Using a resistive heater is optional. In this protocol, we do not present temperature-dependant dynamic detection methods

environment was created to acquire, process, and analyze label-free IRIS images.

1. MATLAB (MathWorks, Natick, MA, USA) (*see* **Note 8**).
2. Curve fitting tool box for MATLAB (MathWorks, Natick, MA, USA) (*see* **Note 9**).

## 3 Methods

### *3.1 Interferometric Reflectance Imaging Sensor*

Here we describe the optical setup of IRIS. The schematic representation is shown in Fig. 3a.

1. Create an optical path with the illuminating LEDs by randomizing the light with a diffuser and then collect the light with a lens. Ensure the diaphragm before the lens is maximized.

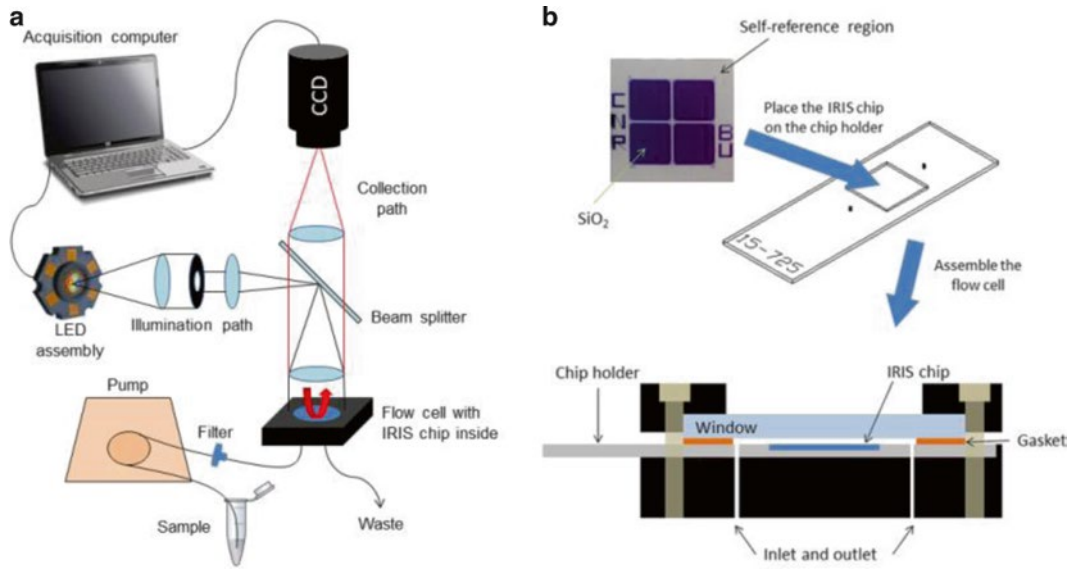


**Fig. 3** The experimental setup of IRIS for dynamic detection. (**a**) The optical setup for IRIS and the related flow components are shown. (**b**) Flow cell assembly is presented

2. With a beam splitter, focus the light beam so that it is directed down to the sample stage and the reflected off the IRIS sensor surface.
3. Use a microscope objective to focus the light beam onto the sensor surface.
4. Collect reflected light from the sample after it has been passed through the objective and then transmitted through the beam splitter.
5. Use a tube lens after the beam splitter to focus the sample image onto a CCD sensor.
6. Iterate through the multiple LEDs via a USB DAQ.

### *3.2 Oligonucleotide Design*

1. Design the oligonucleotide probe to be perfectly complementary to a region of the investigating target while minimizing secondary structure formation (*see* **Note 10**).
2. For detecting SNPs, design the oligonucleotide probe to avoid that the mutation is at a position close to the 5′ or 3′ termini of the probe.
3. Introduce an $NH_2$-modification at the 5′ end of the probes for immobilization on the copoly (DMA-NAS-MAPS) functionalized surface.

The sequences of oligonucleotides used for SNP detection in this work are listed in Table 1.

**Table 1**
**Oligonucleotide sequences used for SNP detection**

| Name | Sequence |
|---|---|
| Target | 5′-TGC AGA CGA CCA GCG GAA AT-3′ |
| PM | 5′-$NH_2$ ATT TCC GCT GGT CGT CTG CA-3′ |
| MM | 5′-$NH_2$ ATT TCC GCT C<u>G</u>T CGT CTG CA-3′ |
| DM | 5′-$NH_2$ ATT TCC C<u>C</u>T GGT C<u>C</u>T CTG CA-3′ |

The underlined nucleotide is the mutation

## 3.3 DNA Microarray Fabrication

### 3.3.1 IRIS Substrate Fabrication

1. Apply S1813 photoresist to a silicon/silicon dioxide wafer by spinning at 2,000 rpm to obtain an approximately 2 μm photopatternable surface layer. Perform a 90 s softbake at 90 °C on a hot plate.
2. Transfer self-reference region pattern with positive hard-contact UV lithography using the MA6 mask aligner with a 30 s exposure.
3. Develop the photoresist in developer for approximately 40 s.
4. Hard bake the photoresist at 120 ° C for 10 min on a hot plate.
5. Etch to the self-reference region using BOE for 7–8 min to expose the silicon surface. The BOE etch rate is approximately 80 nm per minute for thermally grown oxide.
6. Strip photoresist with acetone and sonication (5 min). Rinse in deionized water and then dry. Strip remaining photoresist with oxygen plasma at 300 sccm and 300 W for 2 min.
7. Protect wafer with photoresist, but only perform soft and hard bakes, no exposure or development.
8. Dice wafer into individual dies (chips) using dicing saw. Typical dimensions of chips are 15 mm × 15 mm.
9. Strip photoresist with acetone and sonication (10 min). Rinse in deionized water and then dry. Strip remaining photoresist with oxygen plasma at 300 sccm and 500 W for 5 min. Patterned IRIS chips can be stored indefinitely in a clean environment until use.

### 3.3.2 Surface Functionalization

1. Clean patterned IRIS chips by sonicating in acetone for 5 min, rinsing in methanol, and then rinsing in deionized water. Dry chips with nitrogen gas.
2. Plasma ash the clean IRIS chips with oxygen plasma at 300 sccm and 500 W for 10 min.
3. Prepare 1 % (w/v) copoly (DMA-NAS-MAPS) in a mixture of water and 40 % ammonium sulfate solution (1:1).

4. Place the IRIS chips in the 1 % (w/v) copoly (DMA-NAS-MAPS) solution in a plastic Petri dish and incubate at room temperature for 30 min with shaking (*see* **Note 11**).
5. Rinse the IRIS chips with deionized water, and then wash three times in deionized water for 3 min each on a shaker.
6. Dry the IRIS chips with argon gas, and dry the chips in a vacuum oven at 80 °C for 15 min.
7. Use the chips immediately for microarray printing (*see* **Note 12**).

#### *3.3.3 Oligonucleotide Spotting and Immobilization*

DNA microarrays are fabricated by spotting oligonucleotides on the functionalized IRIS chips with a robotic arrayer (*see* **Note 13**).

1. Design a microarray pattern with at least three replicate spots per oligonucleotide sequence.
2. Set the humidity inside the spotter to 55 % and the temperature of the plate to 20 °C.
3. Spot the oligonucleotide probes at 25 μM concentration in the spotting buffer (1×) on copoly (DMA-NAS-MAPS) functionalized IRIS chips.
4. Upon completion of spotting, keep the DNA microarrays at 70–75 % relative humidity overnight at room temperature.

#### *3.3.4 Washing and Blocking*

1. Wash the IRIS chips in the wash buffer four times for 10 min each in a petri dish on a rotating shaker.
2. Rinse the IRIS chips briefly with deionized water.
3. Incubate the slides with the blocking buffer at room temperature for 1 h.
4. Rinse the chips with deionized water.
5. Dry the chips with argon gas.

### *3.4 Dynamic Label-Free Detection of DNA Hybridization and Denaturation*

A mirror image is acquired to correct for any spatial nonuniformity of illumination on the surface.

#### *3.4.1 Mirror Image Acquisition*

1. Place a silicon mirror (15 mm × 15 mm) in the chip holder and assemble the flow cell as shown in Fig. 3b.
2. Connect all tubing including the filter and place the flow cell on the stage of IRIS for image acquisition, as shown in Fig. 3a.
3. Flow hybridization buffer (1×) through the flow cell.
4. Open acquisition software and turn-on camera.
5. Place a silicon mirror in the field-of-view, then check focus.
6. Set the number of images to be averaged for every illumination source (*see* **Note 14**).
7. Select the maximum exposure time to be used on the camera and ensure that the camera is not being saturated for every illumination source (*see* **Note 15**).

8. Acquire a mirror scan to be used for correcting any spatial nonuniformity.
9. After acquiring the mirror image, disassemble the flow cell and rinse with deionized water and dry.
10. Wash the tubing by flowing 70 % ethanol and then drying (*see* **Note 16**).
11. Clean the window by rinsing with water then carefully wiping with isopropanol and lens cleaning tissue.

#### *3.4.2 Dynamic Image Acquisition for Detecting Hybridization and SNP*

1. Place the IRIS chip in the chip holder and repeat **steps 1–6** described in Subheading 3.4.1. Mirror Image Acquisition.
2. Set the exposure time to be the same as the mirror scan.
3. Set data acquisition software to continuously acquire images.
4. Acquire images for 30 min while hybridization buffer (1×) is flowing to obtain a baseline signal.
5. Introduce DNA targets in hybridization buffer (1×).
6. After hybridization reaches equilibrium, flow diluted hybridization buffer with $[Na^+] = 50$ mM as a wash buffer for 20 min. Use deionized water to dilute the hybridization buffer to reduce the $[Na^+]$ concentration.
7. Introduce diluted hybridization buffer with $[Na^+]$ at a concentration of less than 1 mM. Such ionic strength will start denaturing duplexes at room temperature (*see* **Note 17**).
8. To denature all duplexes and regenerate the microarray, wash it with deionized water.
9. After the experiment is completed, disassemble the flow cell and rinse the flow cell and gasket with deionized water and dry.
10. Clean the window by rinsing with water and then carefully wiping with isopropanol and lens cleaning tissue.
11. Discard the tubing and filter.

### *3.5 Data Processing*

By collecting multispectral data from IRIS chips, it is possible to individually fit each pixel to a reflection curve. This is done by using a nonlinear fitting algorithm available in MATLAB to fit the data to an interferometric model.

1. Data is normalized to the nonuniform spatial illumination as captured by the mirror scan. This is done by dividing the chip image file by the mirror scan for every spectral image collected.
2. To account for temporal variations in illumination power, the data processing software automatically identifies self-reference regions in every image and then divides the intensity measurements by this value, for all wavelengths, to normalize the image [19].

3. Each pixel is then fit to the reflection function that is approximated with the following equation:

$$R = |r|^2 = \frac{r_1^2 + r_2^2 + 2r_1 r_2 \cos(2\phi)}{r_1^2 r_2^2 + 2r_1 r_2 \cos(2\phi)}, \quad (1)$$

where $r_1$ and $r_2$ are the Fresnel reflection coefficients of the air–$SiO_2$ (or buffer–$SiO_2$) and Si–$SiO_2$ interfaces, respectively. The reflection coefficients can be calculated by:

$$r_1 = \frac{n_{ox} - n_1}{n_{ox} + n_1} \text{ and } r_2 = \frac{n_{Si} - n_{ox}}{n_{Si} + n_{ox}}, \quad (2)$$

where $n_1$, $n_{ox}$, and $n_{Si}$ are the refractive indices of air (or buffer solution), $SiO_2$, and Si, respectively. The optical path difference is described by the phase difference, $\phi$, from Eq. 1, which is given by:

$$\phi = \frac{2\pi d}{\lambda} n_{ox} \cos\theta \quad (3)$$

Here, $d$ is the thickness of the layer ($SiO_2$ or $SiO_2$ plus the biomolecule layer), $n_{ox}$ is the refractive index of $SiO_2$, $\lambda$ is the wavelength of the incident light, and $\theta$ is the angle of incidence. The system uses low angles of illumination and collection, therefore the angle of incidence can be assumed to be near zero. The thickness, $d$, is determined by minimizing the error when solving Eqs. 1 and 3 with constants calculated from Eq. 2. Accumulation of biomaterial is measured as an increase in the thickness of this layer.

4. The processing software then generates output files that contain an image of calculated thickness from the previous step as well as fitting error for every pixel.

### 3.6 Data Analysis

#### 3.6.1 Spot Finding/Tracking

Oligonucleotide spots on the surface must be located before they can be analyzed. During the analysis stage, users can manually locate the spots and select the areas used to determine the signal, but manual spot finding may introduce error in the calculation due to user bias. Automating the spot finding algorithm eliminates these effects. Zoiray Technologies developed a software that allows automatic spot finding from a single image. While the software is robust and easy to use, it does not allow automatic spot finding from a stack of images, hence analyzing data by finding spots one image at a time becomes extremely laborious. To avoid this lengthy process, one could identify individual spots from the first image and analyze the same areas for the rest of the images acquired during a single experiment. However, mechanical movements of a

microarray during a dynamic, or real-time, data acquisition caused by the flow system or ambient vibrations can result in fluctuations in the spatial locations of individual spots with respect to the imaging camera. Thus, post-processing software is needed to account for micro-motion of the sensor.

There are two possible strategies to track spots from a stack of images acquired during a real-time experiment. First, image registration techniques can be used. They allow the analysis of the same areas identified from the first image throughout the rest of the experiment by aligning the subsequent images to the first one. Alignment marks on the sensor surface are used to register the images by rotation and lateral translation. While the images can be automatically aligned with 1 pixel resolution, we found that registration performs better if the user manually steps through the translation in sub-pixel increments. Second, an automated spot finding algorithm that can locate every spot for each image throughout the experiment can be used. The automated spot finding algorithm has been shown to be robust to these micro-motions and enables real-time experiments to be analyzed.

While both techniques are capable of tracking individual spots in an automated manner, the spot finding algorithm provides greater accuracy than previous image registration techniques (*see* **Note 18**). Thus, data analysis protocol using the spot finding algorithm is given below [20]. The following analysis is done for the specified field-of-view which can be selected as the entire image if desired. Automatically identified self-reference regions are ignored during analysis.

1. Identify the background by looking at a histogram and identifying the maximum histogram level. This is assumed to be the background level.
2. Specify a level greater than the background. Then perform binary thresholding against the background. The default level is set up as 1 nm.
3. Identify all spots and then eliminate the spots that do not satisfy some basic user settings. These include the minimum and maximum spot sizes as well as symmetry constraint. Any spots that do not satisfy these demands are no longer processed.
4. Calculate the signal as the average value of the background compared to an average value of the center of the spot. These parameters are user specified and correspond to the radii used to find these areas. The spot value, which is defaulted to 80 %, calculates a radius that is smaller than the found spot and then finds the average height in this area. The area is reduced from the edge of the spot to reduce the effect of coffee-ring and other edge behavior. The background area is found by taking an annular ring outside of the spot, as shown in Fig. 4a. The ring values are user specified and default to 120 and 140 %.

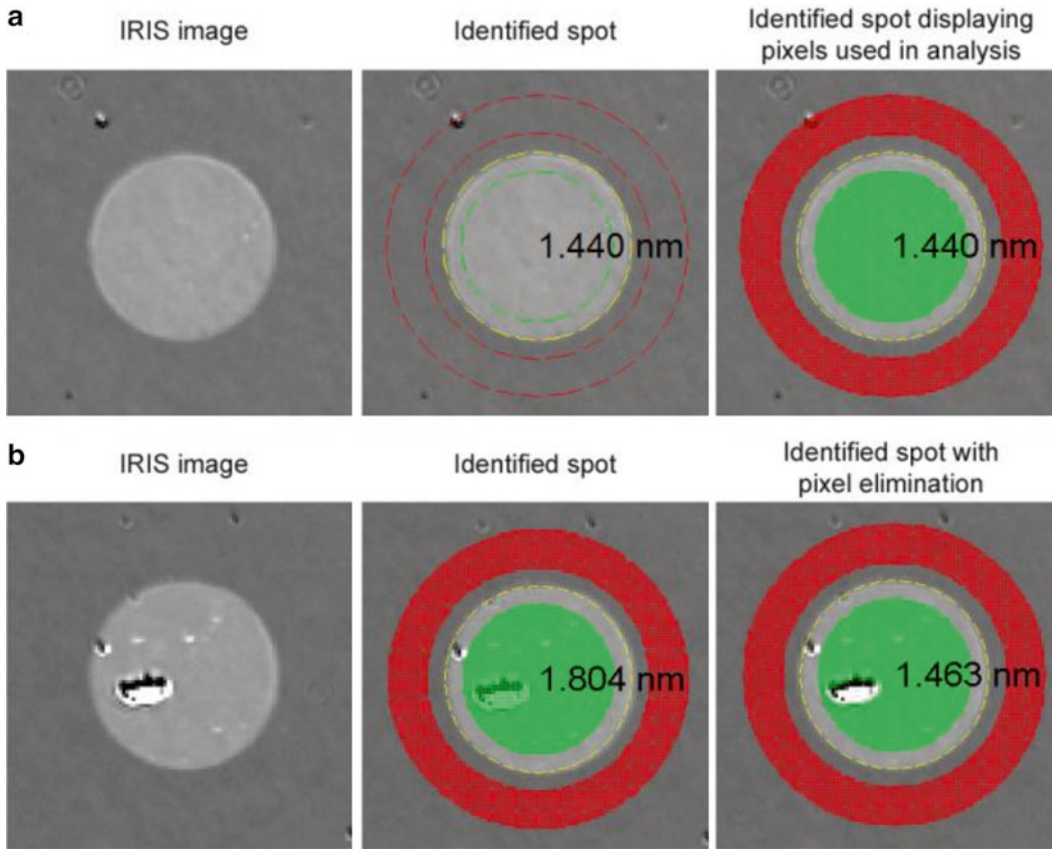


**Fig. 4** Spot finding algorithm. (**a**) A spot, or a sensor, is easily identified by accumulating the vertical and horizontal lines throughout the image. The center and the radius of the sensor are identified as indicated by the *yellow dotted circle*. User specifies the radius inside sensor (*green dotted circle*) as well as the area outside the sensor (*red dotted circles*) to be used as the local background. In this example, a spot height of 1.440 nm was obtained by measuring the differential optical path length of the area defined by 80 % of the sensor radius (*green pixels*) and the area defined by 120 and 160 % of the sensor radius (*red pixels*). (**b**) A spot with a small area artifact, most likely caused by a piece of dirt is analyzed. The *dirt pixels* must be eliminated for accurate quantitative analysis. When only specifying the three radii for the spot finding algorithm, the obtained spot height is 1.804 nm. However, we filtered out all pixels that had fitting error of more than one standard deviation of the entire image. After eliminating the pixels with large error, the obtained spot height is decreased by 19 % to 1.463 nm, a value close to the spot height of a spot without any artifact (the *right image* from (**a**)). As seen in the *right image*, the artifact is not included, and only the *green pixels* are used in calculating the spot height

5. Eliminate undesired pixels using available advanced options. This allows the user to eliminate pixels that fall outside of up to three standard deviations from the median fitting error. In this way, pixels that do not fit well are not included in the calculation of spot or background heights. This often occurs with scratches, dirt, salt, or other undesired artifacts. An example spot using pixel elimination is shown in Fig. 4b.

### 3.6.2 Quantitative Analysis of Hybridization

The spot finding software outputs quantified observations of the sensor, which is the optical path difference of the spot to its background (i.e., spot height). Spot height information can easily be converted into the surface mass density ($\rho_m$) or molecular surface density ($\rho_N$) for quantitative analysis.

1. Obtain surface mass density using the following equation:

$$\rho_m = 0.8\,h, \tag{4}$$

where $\rho_m$ is the surface mass density in ng/mm$^2$, $h$ is the output signal in nm, and 0.8 is the optical density to mass density conversion factor for DNA, which was obtained previously based on using a fixed refractive index model [21].

2. Calculate hybridization efficiency by understanding the molecular surface density of the probe before the hybridization ($\rho_{Np}$) and the molecular surface density of the captured target after hybridization ($\rho_{Nt}$). Molecular surface densities are given by the following equations with the units in number of molecules/mm$^2$.

$$\rho_{Np} = \frac{0.8\times10^{-9}\bullet h_i N_A}{MW_p} \tag{5}$$

$$\rho_{Nt} = \frac{0.8\times10^{-9}\bullet(h'_f - h_i)N_A}{MW_t}, \tag{6}$$

where $N_A$ is Avogadro's number and $MW_p$ and $MW_t$ are molecular weights of the probe and the target, respectively. $h_i$ is the initial spot height (nm) before hybridization and $h'_f$ is corrected height (nm) for refractive index difference between ssDNA and dsDNA, which is given by:

$$h'_f = 0.941\bullet h_f, \tag{7}$$

where $h_f$ is the measured spot height (nm) after hybridization. The correction factor, 0.941, is the ratio of the refractive index of ssDNA ($n\sim1.45$) to that of dsDNA ($n\sim1.54$) [22]. Hybridization efficiency can be calculated by simply taking the ratio of the surface molecular densities of probe and target (divide Eq. 5 by Eq. 6):

$$\%\ \text{Hybridization} = \frac{\rho_{Np}}{\rho_{Nt}}\times100 \tag{8}$$

### 3.6.3 SNP Detection

1. Characterize the denaturation kinetics of different spots by fitting an exponential decay function:

$$f = a_1 e^{(-a_2 t)} + a_3 \tag{9}$$

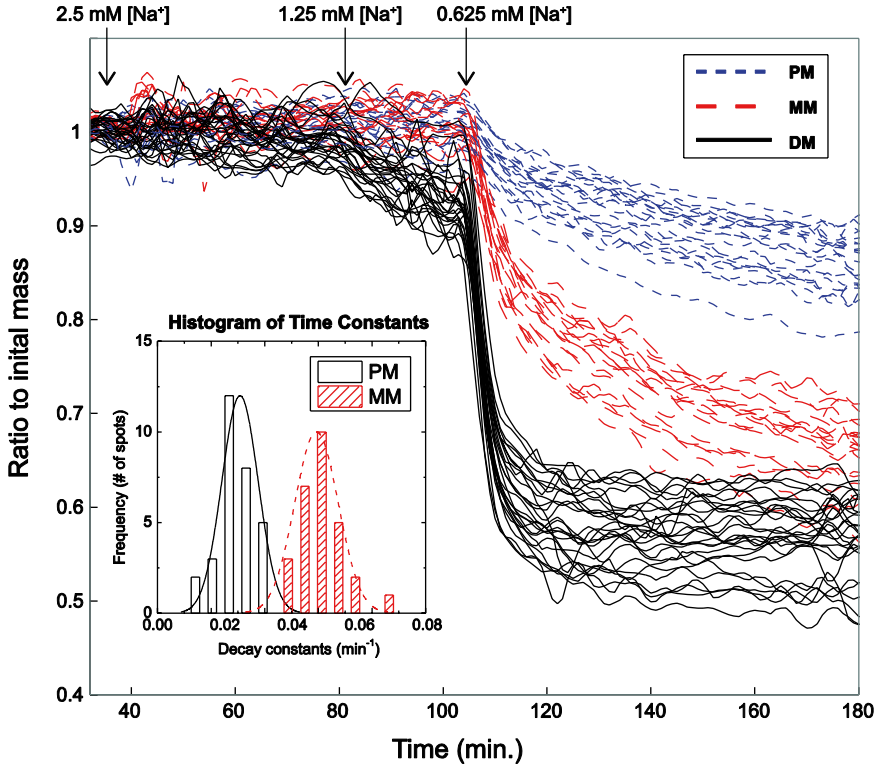


**Fig. 5** Denaturation kinetics of DNA duplexes with and without mutation. Mass change ratio upon the introduction of buffer with low ionic strength is shown. Different duplexes display very different denaturation kinetics (PM-*blue dotted line*, perfect match; MM-*red dash line*, single mismatch; DM-*black solid line*, double mismatch). Single exponential decay functions are fit to mass change ratio of each spot, and the decay constants are shown as a histogram (*inset*). Higher decay constants represent faster denaturation kinetics. The free energy difference ($\Delta G$) between PM and MM is 2.2 kcal/mol, and we can distinguish the two population with 97.2 % CI. The decay constants from the DM probes are too high to be shown in this histogram. This figure was adapted from ref. 16 with permission from Elsevier

While $a_1$ and $a_3$ do not have any experimental significance, they improve the quality of the fitting and do not affect the values found for the decay constant $a_2$. An example of DNA denaturation kinetics is shown in Fig. 5.

2. Plot a histogram of the decay constants. If a mutation is present, the population of the decay constants will have a different distribution from the ones obtained from perfectly complementary duplexes, as shown as an inset in Fig. 5.

## 4 Notes

1. The ACULED VHL LED array is used because the spatial locations of the four different color LEDs are as close as possible. The distance between the LEDs affects the illumination uniformity.

2. Full chemical name of copoly (DMA-NAS-MAPS) is *N*,*N*-dimethylacrylamide(DMA), *N*,*N*-acryloyloxysuccinimide (NAS), and [3-(methacryloyl-oxy) propyl] trimethoxysilyl (MAPS). It can be synthesized as described in refs. [23, 24].
3. One surface of the window has a standard anti-reflection coating for visible and near IR light. The other surface has anti-reflection coating for the same wavelength range, but it is designed for glass–water interface. In addition, the anti-reflection coating is made of a material with very low water solubility to survive aqueous flow experiments. The exact composition of the anti-reflection coating is not disclosed by the manufacturer.
4. The rubber sheet is cut out to make an approximately 50 μL large flow chamber. For the flow cell assembly, the gasket is sandwiched between the IRIS chip and the glass window forming the side walls for the flow chamber.
5. The chip holder is machined out of aluminum to hold IRIS chip in place in the assembled flow cell. The chip holder has the same dimension as a conventional glass slide for easy handling of the IRIS chip. The dimension also allows IRIS chip to be scanned by a conventional microarray fluorescence scanner. Aluminum is chosen as the material of the chip holder because of its good thermal conductivity. It is designed to be placed on top of a resistive heater in an assembled flow cell for temperature control.
6. The top block and the bottom block serve as the main structure. Both pieces are made out of polyoxymethylene (POM), or commercially known as Delrin. POM is the choice of material as it is easy to machine and nonconductive. It also has high heat resistance and low water absorption.
7. The diameter of the tubing determines the flow rate. The inner diameter of the tubing used for the peristaltic pump is 0.04 in., and the inner diameter of the tubing leading to and from the flow cell is 0.03 in.
8. MATLAB is selected as the programming interface because of the familiarity to the developers and because it allows one to easily use many image processing and fitting algorithms. Additionally, all initial modeling is done with MATLAB, allowing rapid testing of new substrate and illuminations designs.
9. Processing, referred to as fitting, can be done using the nonlinear fitting algorithm available in MATLAB's curve fitting toolbox. This process can be computationally demanding, but it is rapidly parallelizable as each pixel can be processed independently. Multi-core processors such as modern graphic processing units (GPU) are ideal for fitting IRIS images. Zoiray Technologies developed fitting software that used GPUs but was difficult to modify. To keep up with the development of

new fitting models, computation time was traded for a reduction in software developer time. To this end, a cluster of computers is used for fitting large numbers of datasets with MATLAB.

10. Possible hairpin structures as well as homodimers and heterodimers of the oligonucleotide probes that can decrease the hybridization efficiency can be calculated with OligoAnalyzer provided by Integrated DNA Technologies (Coralville, IA, USA). The URL for this free software is http://www.idtdna.com/analyzer/Applications/OligoAnalyzer/.
11. Be sure to use a plastic Petri dish for copoly (DMA-NAS-MAPS) coating. A glass container will compete with the IRIS chip for functionalization.
12. The functionalized IRIS chips can be stored in the dessicator for up to 3 weeks. Bake the stored functionalized IRIS chips in a vacuum oven at 80 °C for 15 min prior to spotting.
13. In our work, BioOdyssey Calligrapher MiniArrayer (Bio-Rad, Hercules, CA, USA) was used for oligonucleotide spotting. Alternative arrayers can be used to produce comparable results.
14. Averaging images reduces noise, hence increases the sensitivity of the sensor. However, there is a practical limitation to consider. Averaging 200 images with 0.03 s exposure at every wavelength takes ~30 s to acquire a single data point and result in temporal resolution of greater than 30 s. On the contrary, averaging 20 images with 0.03 s exposure results in temporal resolution of less than 10 s, although the noise will be greater by threefold. The trade-off between the sensitivity and the kinetic characterization capability needs to be considered. In the method we present, we averaged 50 images per wavelength.
15. An ideal target is 80 % of full-well capacity.
16. Make sure the tubing is completely dry to avoid trapping bubbles during the flow experiment.
17. Free energy of the duplexes can be calculated with OligoAnalyzer, as described in **Note 10**, to check the duplex stabilities in different ionic strength buffers.
18. We evaluated the performance of dynamic data processing techniques by analyzing the change in mass density of a protein microarray under a flow for 37 h. The % change in mass density was obtained by using (1) automatic image registration, (2) manual image registration, and (3) spot finding algorithm. The results are compared to the mass density obtained by identifying individual sensors using the software developed by Zoiray Technology. The differences in % change in mass density from using different techniques are presented in Fig. 6. The spot finding algorithm gave a much closer result to the

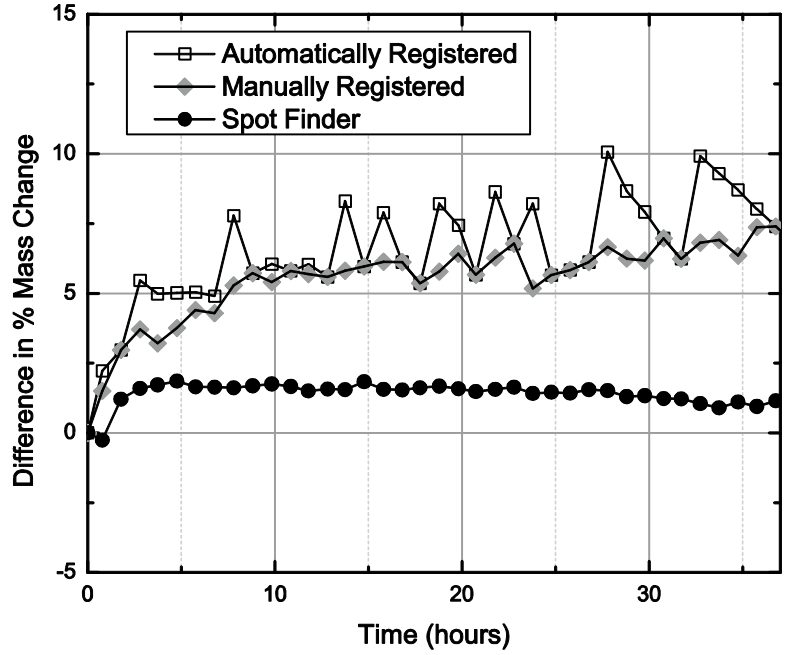


**Fig. 6** Comparison of different methods for dynamic data processing

result obtained using Zoiray Technology's software than image registration techniques did. The average percent difference between the results obtained via the spot finding algorithm from Zoiray's software was $1.4 \pm 2.5$ % with 95 % confidence interval. The average percent difference between the automatic registration and manual registration techniques from Zoiray's software was $6.5 \pm 4.2$ % and $5.5 \pm 4.3$ %, respectively, with 95 % confidence interval. The spot finding algorithm also resulted in the least amount of signal fluctuations throughout the experiment at 0.4 %, whereas the fluctuations from automatic image registration and manual image registration were 2.0 % and 1.5 %, respectively.

## Acknowledgments

We thank Dr. Emre Özkumur for his contributions in developing IRIS and the presented protocol, Professor Marcella Chiari for providing her expertise in surface chemistry, Professor Mario Cabodi for his advice on flow cell design, and Alex Reddington for his help in chip fabrication.

## References


1. Ahn S, Spuhler PS, Chiari M, Cabodi M, Unlum MS (2012) Quantification of surface etching by common buffers and implications on the accuracy of label-free biological assays. Biosens Bioelectron 36:222–229
2. Vignal A, Milan D, SanCristobal M, Eggen A (2002) A review on SNP and other types of molecular markers and their use in animal genetics. Genet Sel Evol 34:275–305
3. Halushka MK, Fan JB, Bentley K, Hsie L, Shen N, Weder A et al (1999) Patterns of single-nucleotide polymorphisms in candidate genes for blood-pressure homeostasis. Nat Genet 22:239–247
4. Gaylord BS, Massie MR, Feinstein SC, Bazan GC (2005) SNP detection using peptide nucleic acid probes and conjugated polymers: applications in neurodegenerative disease identification. Proc Natl Acad Sci USA 102:34–39
5. Kim S, Misra A (2007) SNP genotyping: technologies and biomedical applications. Annu Rev Biomed Eng 9:289–320
6. Peyret N, Seneviratne PA, Allawi HT, SantaLucia J Jr (1999) Nearest-neighbor thermodynamics and NMR of DNA sequences with internal A center dot A, C center dot C, G center dot G, and T center dot T mismatches. Biochemistry 38:3468–3477
7. Fei ZD, Ono T, Smith LM (1998) MALDI-TOF mass spectrometric typing of single nucleotide polymorphisms with mass-tagged ddNTPs. Nucleic Acids Res 26:2827–2828
8. Nicolae DL, Wen XQ, Voight BF, Cox NJ (2006) Coverage and characteristics of the affymetrix GeneChip human mapping 100K SNP set. PLoS Genet 2:665–671
9. Shen R, Fan JB, Campbell D, Chang W, Chen J, Doucet D et al (2005) High-throughput SNP genotyping on universal bead arrays. Mutat Res 573:70–82
10. Zhang SB, Wu ZS, Shen GL, Yu R (2009) A label-free strategy for SNP detection with high fidelity and sensitivity based on ligation-rolling circle amplification and intercalating of methylene blue. Biosens Bioelectron 24:3201–3207
11. Ingebrandt S, Han Y, Nakamura F, Poghossian A, Schoning MJ, Offenhausser A (2007) Label-free detection of single nucleotide polymorphisms utilizing the differential transfer function of field-effect transistors. Biosens Bioelectron 22:2834–2840
12. Rant U, Arinaga K, Scherer S, Pringsheim E, Fujita S, Yokoyama N et al (2007) Switchable DNA interfaces for the highly sensitive detection of label-free DNA targets. Proc Natl Acad Sci USA 104:17364–17369
13. Ozkumur E, Needham JW, Bergstein DA, Gonzalez R, Cabodi M, Gershoni JM et al (2008) Label-free and dynamic detection of biomolecular interactions for high-throughput microarray applications. Proc Natl Acad Sci USA 105:7988–7992
14. Daaboul GG, Vedula RS, Ahn S, Lopez CA, Reddington A, Ozkumur E et al (2011) LED-based interferometric reflectance imaging sensor for quantitative dynamic monitoring of biomolecular interactions. Biosens Bioelectron 26:2221–2227
15. Lopez CA, Daaboul GG, Vedula RS, Ozkumur E, Bergstein DA, Geisbert TW et al (2011) Label-free, multiplexed virus detection using spectral reflectance imaging. Biosens Bioelectron 26:3432–3437
16. Ozkumur E, Ahn S, Yalcin A, Lopez CA, Cevik E, Irani RJ et al (2010) Label-free microarray imaging for direct detection of DNA hybridization and single-nucleotide mismatches. Biosens Bioelectron 25:1789–1795
17. Ahn S, Huang C, Ozkumur E, Zhang X, Chinnala J, Yalcin A et al (2012) TATA binding proteins can recognize nontraditional DNA sequences. Biophys J 103:1510–1517
18. Fish DJ, Horne MT, Searles RP, Brewood GP, Benight AS (2007) Multiplex SNP discrimination. Biophys J 92:L89–L91
19. Vedula R, Daaboul G, Reddington A, Ozkumur E, Bergstein DA, Ünlü MS (2010) Self-referencing substrates for optical interferometric biosensors. J Mod Opt 57: 1564–1569
20. Ahn S, Freedman DS, Massari P, Cabodi M, Ünlü MS (2013) A mass-tagging approach for enhanced sensitivity of dynamic cytokine detection using a label-free biosensor. Langmuir 29:5369–5376
21. Ozkumur E, Yalcin A, Cretich M, Lopez CA, Bregstein DA, Goldberg BB et al (2009) Quantification of DNA and protein adsorption by optical phase shift. Biosens Bioelectron 25:167–172
22. Elhadj S, Singh G, Saraf RF (2004) Optical properties of an immobilized DNA monolayer from 255 to 700 nm. Langmuir 20: 5539–5543
23. Pirri G, Damin F, Chiari M, Bontempi E, Depero LE (2004) Characterization of a polymeric adsorbed coating for DNA microarray glass slides. Anal Chem 76:1352–1358
24. Cretich M, Longhi R, Corti A et al (2009) Epitope mapping of human chromogranin A by peptide microarrays. Methods Mol Biol 570:221–232